DISCRETE AND CONTINUOUS
DYNAMICAL SYSTEMS
Volume **28**, Number **4**, December **2010**

doi:10.3934/dcds.2010.28.1413

pp. **1413–1435**

CHARGE-BALANCED SPIKE TIMING CONTROL FOR PHASE MODELS OF SPIKING NEURONS

Per Danzl, Ali Nabi and Jeff Moehlis

Department of Mechanical Engineering
University of California
Santa Barbara, CA 93106, USA

Abstract. This paper explores event-based feedback schemes for controlling spike timing in phase models of neurons with the constraint of a charge-balanced stimulus over a period of stimulation. We present an energy-optimal control system based on variational methods. We also present a biologically-inspired quasi-impulsive control system that, mimicking the signaling behavior of real neurons, can achieve reference phase tracking. Applied to a pacemaker-driven ensemble, this control can achieve desynchronization using a set of charge-balanced stimuli.

1. **Introduction.** Phase models of neurons have been used to investigate the patterns of synchrony that result from the type and architecture of coupling [6, 17, 10, 24, 1, 19, 16], and the response of large groups of oscillators to external stimuli [7, 8, 36].

Recently, phase models of neurons have also been investigated in the context of controlling neurons to behave in a desired way [36, 30, 13, 11]. Much of the motivation for controlling neurons comes from the desire to treat Parkinson's disease, which causes involuntary tremors around 3-6 Hz that typically affect the distal portion of the upper limbs. These tremors have been associated with the synchronization of a cluster of neurons in the thalamus and basal ganglia [32]. For patients with advanced Parkinson's disease who do not respond to drug therapy, electrical deep brain stimulation (DBS), an FDA-approved therapeutic procedure, may offer relief. In this procedure, a neurosurgeon guides a small electrode into the motor-control region of the brain, and then connects the electrode to a pacemaker-like device implanted in the chest. As presently implemented, the device sends high-frequency (~ 100 Hz) electrical current stimulation pulses directly into the brain tissue, which has been found to alleviate tremors for some patients [4].

There is much interest in designing electrical DBS control systems that use additional electrodes for feedback, thereby making the stimulus "demand-controlled" [36, 37]. A feedback-based approach is attractive from a clinical perspective in that the biological tissue is only stimulated when necessary, thereby reducing the overall accumulation of negative side effects of electrical stimulation, and also the amount of power required from the implanted battery. There are, however, challenges to implementing feedback control for neurons. First, the conductance-based formalism first proposed by Hodgkin and Huxley in [20], a general modeling methodology in neuroscience, yields systems of continuous-time ordinary differential equations that

2000 *Mathematics Subject Classification.* Primary: 92C20, 93C15; Secondary: 37N25.
Key words and phrases. Mathematical neuroscience, control, phase models.

tend to be *highly* nonlinear. Many traditional feedback control system designs require the controlled system to be either linear or only *weakly* nonlinear. A second challenge is that a control scheme cannot stimulate biological tissue with arbitrarily large signals. The magnitude of the electrical stimulus must be constrained to acceptable ranges for hardware implementation and biological tissue tolerance. A third challenge is the fact that the only state that is directly observable is the neuron's membrane voltage. A control system cannot measure the dynamic states of the many ion channels that play a critical role in the oscillatory behavior of neural spiking. This poses particular problems for implementing traditional nonlinear feedback control systems, which depend on continuous measurements of state [23]. The control algorithms in this paper are intended to at least partially overcome these challenges.

We will focus on feedback control of neurons modeled by the Hodgkin-Huxley equations, which display many of the dynamical characteristics of real oscillatory neurons, and constitute the most widely studied model in mathematical neuroscience. The Hodgkin-Huxley model possesses regimes in which the oscillatory spiking can be either advanced or retarded by unipolar stimulation pulses, depending on the time of injection. Also, the Hodgkin-Huxley model exhibits *Class 2 neural excitability*, which means that there is a bistable bifurcation structure featuring a subcritical Hopf bifurcation that leads to a discontinuous relationship between injected baseline current and firing frequency [22]. This model, while not representing human brain neurons, is the prototypical model for neuronal membrane dynamics, and exhibits oscillatory behavior similar to human motor control neurons in the thalamus and basal ganglia regions of the brain. Due to this qualitative similarity, and the fact that the Hodgkin-Huxley model is perhaps the most widely studied and familiar conductance-based neuron model, we choose to consider it as our neuron model in this paper. Such conductance-based models are amenable to generating control schemes that are experimentally realizable *in vitro*, as shown in recent work [34].

Our control algorithms are designed to achieve charge balance, i.e. the net electrical charge injected into a neuron over one control cycle is equal to zero. This is important because accumulation of charge leads to irreversible Faradiac reaction products that cause neural tissue damage [28]. There is a trade-off, however. Charge-balanced stimulation has been shown to cause less tissue damage [26, 27], but increases the likelihood of corrosion damage of the stimulating electrode, an issue currently being addressed by materials science and microelectronics research [28]. We focus on charge-balance in the hope that developments in electrode design technology will mitigate the corrosion problem.

As mentioned above, the only observable state is the neuron's membrane voltage. In practice, background noise often affects the voltage measurement to the extent that the only reliable observation is the detection of voltage spikes, rather than the instantaneous value of the voltage itself. This situation leads us to employ a control methodology known as *event-based control*. The concept of event-based control, sometimes known as Lebesgue sampling, was developed as an improvement to fixed sample-rate feedback control for digital systems [2]. As shown in previous work [13, 14], this methodology finds natural utility in systems involving spiking neurons. In particular, rather than developing a control law based on continuous voltage feedback, we will focus on observing the voltage spikes as *events*. This event-based framework is convenient because we can consider the spike timing objective as

an event-timing objective. Much work on event-based control of nonlinear systems has been done, especially with respect to stochastic processes [3]. While we do not consider stochasticity here, the event-based framework is well-suited to overcoming the observability and nonlinearity challenges inherent in spike timing control of oscillatory neurons.

The organization of the paper is as follows. After introducing the conductance-based modeling framework and how a phase reduction procedure can be used to simplify the system in Section 2, we consider several different objectives and methods for controlling neurons. In Section 3, we consider the control of an individual neuron, first finding the energy-optimal stimulus which causes a neuron to fire at a specified time, then controlling a neuron to fire at the times given by a reference oscillator using impulsive and quasi-impulsive inputs. In Section 4, we describe how these methods might be extended to control an ensemble of neurons, including a population driven by a pacemaker. We give concluding remarks in Section 5.

2. Models.

2.1. Conductance-based models.

The membrane dynamics of neurons can be represented using a conductance-based formalism, in space-clamped form, yielding a system of ordinary differential equations of the form:

$$c\dot{V} = I_g(V,\mathbf{n}) + I_b + I(t), \quad \dot{\mathbf{n}} = \mathbf{G}(V,\mathbf{n}), \tag{1}$$

where $V \in \mathbb{R}$ is the voltage across the membrane, $\mathbf{n} \in \mathbb{R}^d_{[0,1]}$ is the vector of gating variables which correspond to the state of the membrane's ion channels, $c \in \mathbb{R}^+$ is the constant membrane capacitance, $I_g : \mathbb{R} \times \mathbb{R}^d \mapsto \mathbb{R}$ is the sum of the membrane currents, and $I : \mathbb{R} \mapsto \mathbb{R}$ is the stimulus current. $I_b \in \mathbb{R}$ is the baseline current, which represents the effect of other parts of the brain on the neuron under consideration and can be viewed as a bifurcation parameter in the model that controls whether the neuron is in an excitable or an oscillatory regime. This form of ODE representation was first employed by Hodgkin and Huxley to model the *Loligo* squid's giant axon [20], for which they considered three gating variables (i.e., $d = 3$). We reproduce the specifics of this model:

$$\begin{aligned}
\dot{V} &= (I_b + I(t) \overbrace{-\bar{g}_{Na} h (V - V_{Na}) m^3 - \bar{g}_K (V - V_K) n^4 - \bar{g}_L (V - V_L)}^{I_g(V,\mathbf{n})})/c \,, \\
\dot{m} &= a_m(V)(1-m) - b_m(V) m \,, \\
\dot{h} &= a_h(V)(1-h) - b_h(V) h \,, \\
\dot{n} &= a_n(V)(1-n) - b_n(V) n \,,
\end{aligned}$$

$$\begin{aligned}
a_m(V) &= 0.1(V+40)/(1-\exp(-(V+40)/10)) \,, \\
b_m(V) &= 4\exp(-(V+65)/18) \,, \\
a_h(V) &= 0.07\exp(-(V+65)/20) \,, \\
b_h(V) &= 1/(1+\exp(-(V+35)/10)) \,, \\
a_n(V) &= 0.01(V+55)/(1-\exp(-(V+55)/10)) \,, \\
b_n(V) &= 0.125\exp(-(V+65)/80) \,,
\end{aligned}$$

$$V_{Na} = 50 \text{ mV} \,,\ V_K = -77 \text{ mV} \,,\ V_L = -54.4 \text{ mV} \,,\ \bar{g}_{Na} = 120 \text{ mS/cm}^2 \,,$$
$$\bar{g}_K = 36 \text{ mS/cm}^2 \,,\ \bar{g}_L = 0.3 \text{ mS/cm}^2 \,,\ c = 1 \ \mu\text{F/cm}^2.$$

Control of the spike timing of this system is non-trivial due to the fact that I_g and $\mathbf{G}$ are highly nonlinear and the gating variables $\mathbf{n} = [m, h, n]^{\mathrm{T}}$ are not observable by the controller. We therefore seek a simpler representation of the dynamics of this model that will capture its fundamental behavior, but is amenable to analysis.

2.2. **Phase reduction and phase models.** Generally, in the case of oscillatory synchronization, the participating neurons fire periodically, corresponding to a region of I_b parameter space where the ODEs (1) have a stable periodic orbit. Following [7], we define $\mathbf{x} \equiv [V, \mathbf{n}^{\mathrm{T}}]^{\mathrm{T}}$ so that we can conveniently represent the entire state of the full-dimensional model in one vector. We introduce the phase variable $\theta \in [0, 2\pi) \cong \mathbb{S}^1$ which parametrizes the position of the state on its periodic orbit $\mathbf{x}^{\mathrm{P}}(\theta)$. Using the concept of isochrons [18], this notion of phase can be extended to all points in the basin of attraction of the periodic orbit. By convention, $\theta = 0$ corresponds to the point on the periodic orbit associated with the neuron firing, which is the point of maximum voltage. In the absence of input, the system simply evolves along $\mathbf{x}^{\mathrm{P}}(\theta)$ with constant frequency ω. In general, the phase-reduced dynamics obey the ODE [7]

$$\dot{\theta} = \omega + \mathbf{Z}(\theta) \cdot \mathbf{u}(t),$$

where the phase response curve $\mathbf{Z}(\theta)$ and the input $\mathbf{u}(t)$ are vector functions of the same dimension as the original system (1). However, since the electrical stimulus $I(t)$ affects only the voltage direction of the dynamics (1), we have $\mathbf{u}(t) = [I(t)/c, \mathbf{0}_{1\times d}]^T$, so only the first component of $\mathbf{Z}(\theta)$ comes into play. Thus we obtain the phase-reduced model

$$\dot{\theta} = \omega + Z(\theta)u(t), \tag{2}$$

where $Z(\theta) = \mathbf{Z}_V(\theta)$ is the voltage component of the phase response curve, which essentially captures the effect of impulsive perturbations in the voltage on the phase variable, and $u(t)$ is the input current $I(t)$ normalized by the membrane capacitance c. We note that hereafter we will refer to the scalar $Z(\theta)$ as the phase response curve (PRC). The phase-reduced model is valid in a neighborhood of the periodic orbit where perturbations off $\mathbf{x}^{\mathrm{P}}(\theta)$ are asymptotically attracted back with a phase-shift dictated by isochrons, as described in [38] and summarized in [7].

We note that the Hodgkin-Huxley model is categorized as a Type II neuron model in the neuroscience literature [21]. Type II neuron models are those for which the PRCs have both positive and negative regions, and are typically associated with the neuron model having a Hopf (or Bautin) bifurcation [7]. For the Hodgkin-Huxley model, we take $I_b = 10$ mA to ensure the existence of a stable periodic orbit. We also note that in the absence of stimuli, this stable periodic orbit has a natural frequency of $\omega = 0.43$ rad/ms [33]. The Hodgkin-Huxley model yields a PRC which is shown in Figure 1 and labeled with the following important points:

$$\begin{array}{rclcrcl} \alpha & = & \operatorname{argmin}(Z(\theta)) & , & Z_{min} & = & Z(\alpha) \\ \beta & = & \operatorname{argmax}(Z(\theta)) & , & Z_{max} & = & Z(\beta). \end{array}$$

In general, PRCs for Type II neurons are characterized by the following conditions:

$$\begin{array}{rclcrcl} Z(0) & = & 0 & , & Z'(0) & < & 0 \\ Z(\gamma) & = & 0 & , & Z'(\gamma) & > & 0 \\ Z_{max} & > & 0 & , & Z_{min} & < & 0 \end{array}$$
$$0 < \alpha < \gamma < \beta < 2\pi. \tag{3}$$

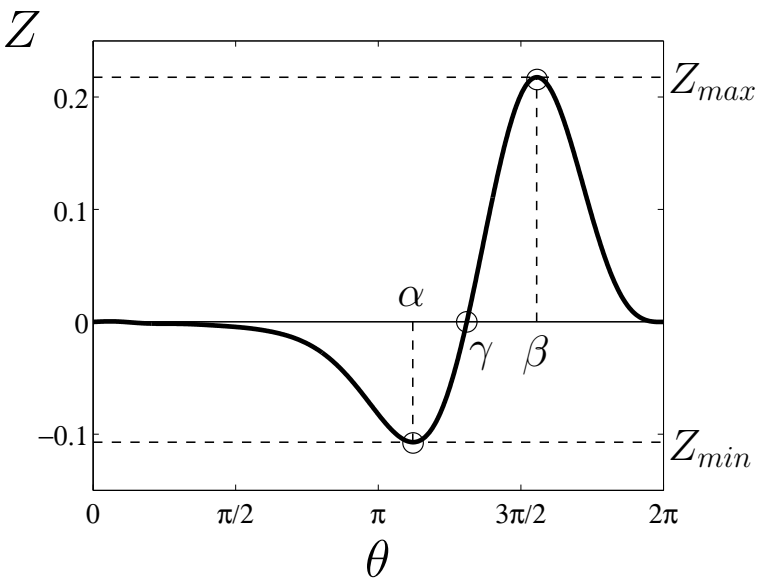

FIGURE 1. Phase response curve computed for the Hodgkin-Huxley neuron model for $I_b = 10$mA.

3. **Control of individual neurons.** In this section we consider the control of an individual neuron, first finding the energy-optimal charge-balanced current which causes a neuron to fire at a specified time, then controlling a neuron to fire asymptotically in-phase with a reference oscillator using charge-balanced impulsive and quasi-impulsive inputs.

Energy-optimal control by the Euler-Lagrange method is a classical control methodology particularly well-suited to nonlinear systems including phase models like (2) [30]. We begin this section by applying this method with the addition of a charge-balance constraint to generate stimulus waveforms that dictate the firing time of the controlled neuron.

3.1. **Energy-optimal spike timing control.** Here we present an event-based control scheme that, after detecting a spike at time t^*, stimulates the neuron with a pre-computed charge-balanced energy-optimal waveform in order to drive the neuron to spike next at a given time $t_1 > t^*$. Without loss of generality, we can take $t^* = 0$.

Consider the phase model (2) for a spiking neuron augmented by an additional dynamic state q:

$$\begin{aligned} \dot{\theta} &= \omega + Z(\theta)u(t), \\ \dot{q} &= u(t), \\ \theta(0) &= 0, \\ q(0) &= 0, \end{aligned} \tag{4}$$

where q is simply the integral of the total stimulus delivered to the neuron [31]. In order to achieve charge balance, q must equal zero after the control waveform is applied.

The total input energy to the system is the integral of the square of the input stimulus over the time horizon of $[0, t_1]$, scaled by the equivalent circuit impedance. The optimality criterion is to minimize this total input energy. So, for a specified spike time t_1, from the set of all stimuli $u(t)$ which evolve $\theta(t)$ via (2) from $\theta(0) = 0$ to $\theta(t_1) = 2\pi$, we want to find the stimulus which minimizes the following cost function:

$$\mathcal{G}[u(t)] = \int_0^{t_1} [u(t)]^2 \mathrm{d}t, \tag{5}$$

and yields $q(t_1) = 0$. Other optimality criteria lead to other cost functions, but can be handled similarly (cf. [9]).

We apply calculus of variations to minimize [15]

$$\mathcal{C}[\mathbf{\Phi}(t), \dot{\mathbf{\Phi}}(t), u(t)] = \int_0^{t_1} \underbrace{\left\{ [u(t)]^2 + \begin{bmatrix} \lambda_1(t) & \lambda_2(t) \end{bmatrix} \cdot \begin{bmatrix} \omega + Z(\theta)u(t) - \dot{\theta} \\ u(t) - \dot{q} \end{bmatrix} \right\}}_{\mathcal{L}[\mathbf{\Phi}, \dot{\mathbf{\Phi}}, u(t)]} \mathrm{d}t, \tag{6}$$

where $\mathbf{\Phi}(t) = [\theta(t),\ q(t),\ \lambda_1(t),\ \lambda_2(t)]^T$. The Lagrange multipliers $\lambda_1(t)$ and $\lambda_2(t)$ force the dynamics to satisfy (4).

Using vector notation, the associated Euler-Lagrange equations are:

$$\frac{\partial \mathcal{L}}{\partial u} = \frac{d}{dt}\left(\frac{\partial \mathcal{L}}{\partial \dot{u}}\right), \qquad \frac{\partial \mathcal{L}}{\partial \mathbf{\Phi}} = \frac{d}{dt}\left(\frac{\partial \mathcal{L}}{\partial \dot{\mathbf{\Phi}}}\right),$$

so that

$$u(t) = -\frac{\lambda_1(t)Z(\theta) + \lambda_2(t)}{2}, \tag{7}$$

$$\dot{\theta} = \omega - \frac{\lambda_1(t)[Z(\theta)]^2 + \lambda_2(t)Z(\theta)}{2}, \tag{8}$$

$$\dot{q} = u(t) = -\frac{\lambda_1(t)Z(\theta) + \lambda_2(t)}{2}, \tag{9}$$

$$\dot{\lambda}_1 = \frac{[\lambda_1(t)]^2 Z(\theta)Z'(\theta) + \lambda_1(t)\lambda_2(t)Z'(\theta)}{2}, \tag{10}$$

$$\dot{\lambda}_2 = 0, \tag{11}$$

where $' = d/d\theta$. To find the optimal $u(t)$, (8)-(11) need to be solved subject to the conditions

$$\theta(0) = 0, \quad \theta(t_1) = 2\pi, \qquad q(0) = 0, \quad q(t_1) = 0. \tag{12}$$

This is a two point boundary value problem where the boundary values for $\theta(t)$ and $q(t)$ are given in (12). The solution of this boundary value problem is aided by the following theorem, which is related to Proposition 2.3 from [30].

Theorem 3.1. *Suppose $Z(0) = 0$ and $\omega > 0$, as is commonly the case for neuron models. Then, for given values t_1 and λ_2, there is a unique trajectory solving the Euler-Lagrange equations (8)-(11) with boundary conditions (12).*

Proof. From (11), λ_2 is a constant. Therefore, for the 2-dimensional system (8), (10) the Hamiltonian

$$h(\theta, \lambda_1) = \lambda_1(t)\omega - \frac{[\lambda_1(t)]^2[Z(\theta)]^2}{4} - \frac{\lambda_1(t)\lambda_2 Z(\theta)}{2} \tag{13}$$

is conserved along the solutions $(\theta(t), \lambda_1(t))$. Letting

$$h_0 = h(\theta(0), \lambda_1(0)) = h(0, \lambda_1(0)),$$

we have

$$\lambda_1(t)\omega - \frac{[\lambda_1(t)]^2[Z(\theta)]^2}{4} - \frac{\lambda_1(t)\lambda_2 Z(\theta)}{2} - h_0 = 0. \tag{14}$$

We first demonstrate that

$$\frac{d\theta}{dt} > 0, \tag{15}$$

as follows. Consider a trajectory $\{(\theta(t), \lambda_1(t))\}$, $0 \le t \le \tau$ with $\theta(\tau) = 2\pi$ and which solves (8),(10). From (8), we have $\frac{d\theta}{dt}|_{t=0} > 0$. Now assume in point of contradiction that there exists a time $0 < \hat{t} < \tau$ such that $\frac{d\theta}{dt}|_{t=\hat{t}} < 0$. Since $\theta(\tau) = 2\pi$, in this case there also exists a phase $\bar{\theta} < 2\pi$ such that $\theta(t) = \bar{\theta}$ for three distinct times between 0 and τ. A quick sketch in the (θ, λ_1) plane shows that, since any trajectory $\{(\theta(t), \lambda_1(t))\}$ is not self-intersecting, the trajectory under our assumption contains three distinct points $(\bar{\theta}, \lambda_1^{(j)})$, $j = 1, 2, 3$. However, the trajectory must also be a level set of the Hamiltonian; from (14), which is quadratic in λ_1, such a level set contains at most two points (θ, λ_1) for any value of θ. Therefore, a contradiction has been reached, and (15) follows.

Now, multiplying (14) by $[Z(\theta)]^2$ and rearranging we get

$$\left([\lambda_1(t)][Z(\theta)]^2\right)^2 + (2\lambda_2 Z(\theta) - 4\omega)\left(\lambda_1(t)[Z(\theta)]^2\right) + 4h_0[Z(\theta)]^2 = 0.$$

Solving for $\lambda_1(t)[Z(\theta)]^2$ yields

$$\lambda_1(t)[Z(\theta)]^2 = -(\lambda_2 Z(\theta) - 2\omega) \pm \sqrt{(\lambda_2 Z(\theta) - 2\omega)^2 - 4h_0[Z(\theta)]^2}. \tag{16}$$

From (8) and (15), $\lambda_1(t)[Z(\theta)]^2 < -(\lambda_2 Z(\theta) - 2\omega)$. Thus, in (16) the valid solution is the *minus* branch, i.e.,

$$\lambda_1(t)[Z(\theta)]^2 = -(\lambda_2 Z(\theta) - 2\omega) - \sqrt{(\lambda_2 Z(\theta) - 2\omega)^2 - 4h_0[Z(\theta)]^2}. \tag{17}$$

Now, from (8) we can write

$$\begin{aligned} t_1 = \int_0^{t_1} dt &= \int_0^{2\pi} \frac{d\theta}{\omega - \frac{\lambda_1(t)[Z(\theta)]^2 + \lambda_2 Z(\theta)}{2}} \\ &= \int_0^{2\pi} \frac{d\theta}{\sqrt{\left(\frac{\lambda_2 Z(\theta)}{2} - \omega\right)^2 - h_0[Z(\theta)]^2}}, \end{aligned} \tag{18}$$

where the last equality uses (17). Differentiating with respect to h_0, gives

$$\frac{dt_1}{dh_0} = \frac{1}{2}\int_0^{2\pi} \frac{[Z(\theta)]^2 d\theta}{\left[\left(\frac{\lambda_2 Z(\theta)}{2} - \omega\right)^2 - h_0[Z(\theta)]^2\right]^{3/2}} > 0, \tag{19}$$

Therefore, t_1 increases monotonically with h_0. Also, from (13), $h_0 = h(\theta(0), \lambda_1(0))$ $= h(0, \lambda_1(0)) = \omega\lambda_1(0)$. So t_1 increases monotonically with $\lambda_1(0)$. This means that, for a given t_1 and λ_2, there is a unique value of $\lambda_1(0)$, which gives a unique trajectory. □

A shooting method is used to solve this boundary value problem numerically. We choose an arbitrary nonzero value of λ_2, take $\theta(0) = q(0) = 0$, and solve the system (8)-(11) iteratively for different nonzero guesses of $\lambda_1(0)$ until $\theta(t_1) = 2\pi$ with a predefined tolerance. Once an upper and a lower bound for $\lambda_1(0)$ is found, employing the bisection method guarantees an answer. From Theorem 3.1, there is a unique $\lambda_1(0)$ that satisfies this. After finding this $\lambda_1(0)$ and its associated trajectory

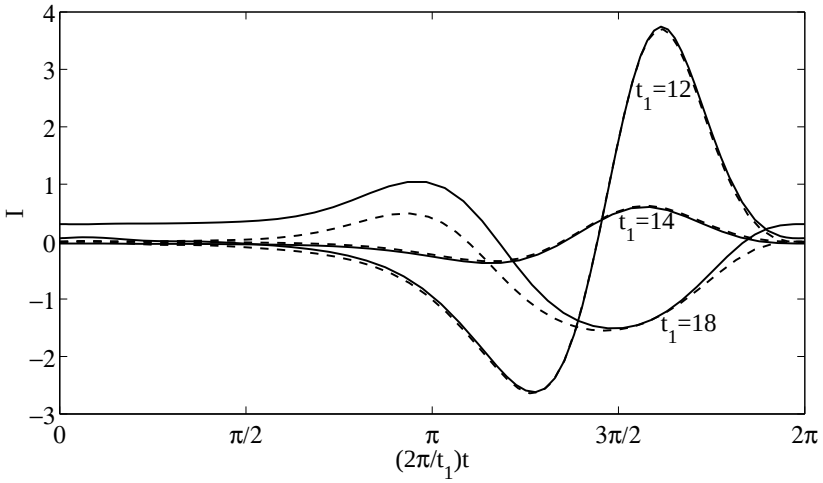

FIGURE 2. Hodgkin-Huxley phase neuron model energy-optimal current for three different values of t_1 with (solid lines) and without (dashed lines) the charge-balance constraint.

numerically, we check if the resulting $q(t_1)$ is within a small tolerance of 0. If so, the problem is considered solved. If not, we conclude that our original choice for λ_2 had been wrong and so a new value is chosen for λ_2 using the bisection method, and the process is repeated. The next choice of λ_2 is made by examining the $q(t_1)$ error gradient from the previous two simulations. The procedure continues until a pair $(\lambda_1(0), \lambda_2)$ is found for which the boundary conditions in (12) are achieved. A consequence of Theorem 3.1 is that we can effectively search for a solution to the Euler-Lagrange equations along a one-dimensional curve in $(\lambda_1(0), \lambda_2)$ space.

Once the optimal trajectories for $\theta(t)$ and $\lambda_1(t)$ are found, we can find the optimal control input by evaluating (7). The solid lines in Figure 2 show the charge-balanced optimal inputs to the system for different t_1's. Recall that we have assumed the neuron's capacitance to be $c = 1$ for these simulations, and thus the optimal input is actually an electrical current stimulus, as indicated in this figure. Note that the horizontal axis in this figure is scaled for ease of comparison.

By removing the charge-balance constraint we reproduce the results of [30]. In this case $\lambda_2 \equiv 0$, hence eliminating the charge-balance constraint. Again the shooting method is used to find the $\lambda_1(0)$ that would result in $\theta(t_1) = 2\pi$. The results for the optimal currents for this case are shown by the dashed lines in Figure 2. In this case, the optimal currents all start and end at zero, whereas in the case with the charge-balance constraint, they do not. It is worth pointing out that considering the phase-reduced model (2) and the shape of the PRC in Figure 1, one can easily verify the shape of achieved currents. The natural period of oscillations for this model is $T = 14.63$ ms. Therefore, for spike times $t_1 < T$ one needs to increase $\dot{\theta}$ in (2). Since the objective is to minimize the input energy, intuitively, one would expect the sign of the currents to approximately follow the PRC's sign to make maximum use of the injected current. Conversely, for $t_1 > T$, one expects to achieve currents with signs opposite to that of the PRC's in most of the time. The currents in Figure 2 justify this argument. In fact, when the charge balance

constraint is not imposed, the optimal currents take the exact same (resp. opposite) sign of the PRC for $t_1 < T$ (resp. $t_1 > T$).

We note that it has been proven in [30] that in the case of no charge-balance constraint, the optimal solutions always exist and are unique. Furthermore, it was shown analytically that for small $|t_1 - T|$, the optimal current $I(t)$ approximately takes the shape of the PRC (shown in Figure 1).

Theoretically, given (2), one can achieve an optimal control input for any desired t_1. However, a constraining factor is the range of validity of the phase-reduced model for the large stimulus waveforms necessary to obtain extreme values of t_1. As mentioned in Section 2.2, the phase-reduced model is only valid when the stimuli are small, meaning the system is in a close neighborhood of the periodic orbit. Therefore, for large values of $|t_1 - T|$ that require large stimuli, the phase-reduced model may not yield accurate results. In addition, there are practical limitations for the level of the current stimulus based on the capability of the hardware in delivering the current and the endurance of the biological tissue immediate to the injection probe, as was discussed in Section 1. We remark that the method presented in this section has also been applied to neurons with Type I PRCs [31].

We will now turn our attention to a set of control schemes that are inspired by the signals used by real neurons and are useful for driving the controlled neurons to spike in phase with a given reference oscillator.

3.2. **Reference-phase tracking.** Consider instead the objective of controlling a neuron to spike (asymptotically) in phase with a reference oscillator with the same natural period as the neuron. The reference oscillator evolves according to the simple equation

$$\dot{\theta}_r = \omega_r \quad , \quad \theta_r(0) = \theta_{r_0}, \tag{20}$$

where $\omega_r = \omega$ is the natural frequency of the reference oscillator, and θ_{r_0} is its initial phase. We will see later in Sections 4.1.2 and 4.2 that such a control objective can be useful for controlling an ensemble of synchronized phase neurons to desynchronize by driving each neuron to follow a staggered reference phase trajectory.

The times at which the phase of the reference oscillator crosses zero are the times we want the controlled phase neuron to spike. To achieve this, we must develop a control scheme that, after every event-based open-loop stimulus application, drives the controlled neuron to spike closer (in time) to the zero crossing of the reference oscillator. One can think of the difference in the time at which the controlled neuron spikes to the time that the reference oscillator crosses zero as a *time error*. From a control-theoretic perspective, this is equivalent to the *phase error* at the time of the controlled neuron's spike. When the controlled neuron spikes, we compare its phase to that of its reference oscillator, and construct an open-loop waveform that will actuate the neuron with the goal of correcting all, or a portion of, its phase error by the time the neuron spikes again.

Generally, one would define the phase error as

$$\Delta\theta = \theta - \theta_r.$$

In the scenario presented in this paper, the phase error is sampled only when the controlled neuron spikes, i.e. $\theta = 0$, so effectively $\Delta\theta = -\theta_r$. However, the phase error, as defined this way, exists on $(-2\pi, 0]$. The topology of the unit phase circle allows us to wrap the phase error to the interval $(-\pi, \pi]$ using the following

algorithm (shown here in general form):

$$\Delta\theta = \begin{cases} \theta - \theta_r & , \quad \text{for} \quad |\theta - \theta_r| \leq \pi \\ \theta - \theta_r - \text{sgn}(\theta - \theta_r)2\pi\,, & \quad \text{for} \quad |\theta - \theta_r| > \pi \end{cases} \tag{21}$$

so that the phase error is the shortest distance around the unit phase circle.

When $\Delta\theta < 0$, the controller should speed up the neuron, and when $\Delta\theta > 0$ it should slow down the neuron. This definition of phase error is useful from the perspective of controlling oscillatory neurons. Figure 3 illustrates why this definition of phase error is appropriate. The reference oscillator trajectories are shown in dashed lines. The time at which the controlled neuron spikes and triggers the event-based controller is labeled t_0. The left panel shows a scenario wherein $\Delta\theta < 0$. With this definition of phase error, the controller should seek to drive the controlled neuron to spike at the time labeled t_r, thus speeding it up. The right panel shows a scenario where $\Delta\theta$ is small and slightly positive. If the phase error was not wrapped, for an arbitrarily small error, the controller would try to make the neuron spike almost immediately, which would require a very strong stimulus. Instead, with the phase error wrapping algorithm, the controller's objective is to slow down the neuron using a small stimulus so that the controlled neuron spikes in phase with the reference neuron one period later, as shown by the marker at t_r on the right panel of Figure 3.

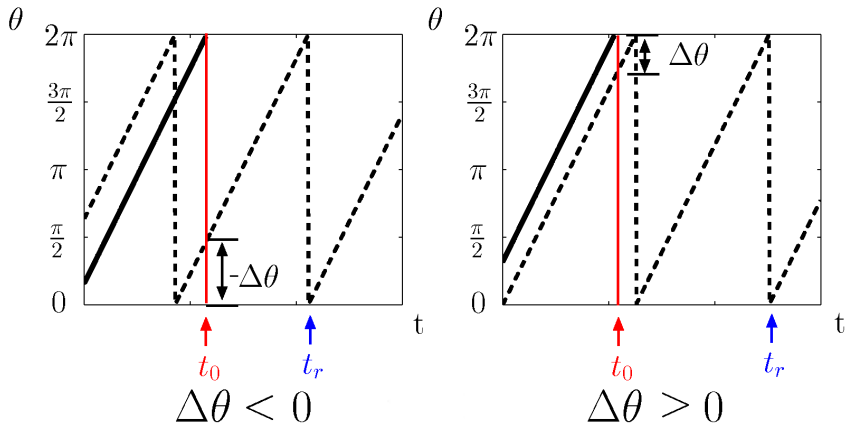

FIGURE 3. Phase error sign convention examples. Reference trajectories are shown as dashed lines. The controlled neuron's phase is shown as a solid line. When the controlled neuron's phase reaches $2\pi = 0 \pmod{2\pi}$, it spikes and triggers assessment of phase error relative to the reference oscillator.

In this event-based framework, we are interested in how the phase error $\Delta\theta$ changes after a period of control actuation, so we will define $\Delta\theta^+$ to be the phase error at the time of the next spiking event. Thus, we seek a control law that decreases the phase error over one period, i.e. ,

$$\left|\frac{\Delta\theta^+}{\Delta\theta}\right| < 1 \quad \forall\ \Delta\theta \in (-\pi, \pi],$$

excluding $\Delta\theta = 0$ (where $\Delta\theta^+$ should also equal 0).

We will begin by describing a heuristic approach, inspired by the way real neurons behave in biological systems, that is both mathematically tractable and intuitive.

3.2.1. *Impulsive control.* In contrast to the continuous time smooth energy-optimal inputs considered in Section 3.1, here we seek to achieve reference phase tracking by using impulsive control signals. In nature, neurons communicate by voltage spikes that are large in magnitude but very short in duration, which naturally limits the production of irreversible Faradaic reaction products that can lead to tissue damage [28]. Signals of this kind are a biological analog of impulses. In fact, dynamical systems researchers in mathematical neuroscience have long used the concept of impulsive coupling to model networks of neurons, see e.g. [5]. Impulsive coupling has been shown to closely correspond to many types of oscillatory biological networks in nature [29, 39]. This has inspired the idea of using impulsive signals (Dirac delta functions) for spike timing control. Impulses are analytically desirable inputs from the perspective of the phase-reduced model, since delta functions turn the calculus into simple algebra. For example, consider the dynamics of generic phase-reduced model over the time interval $[t_I, t_{II}]$ subject to an impulsive input at time $\hat{t}$

$$\dot{\theta} = \omega + Z(\theta)\tilde{u}\delta(t - \hat{t}),$$

where $t_I \leq \hat{t} < t_{II}$, and $\tilde{u}$ is the strength of the impulsive stimulus. The solution is simply

$$\theta(t_{II}) = \theta(t_I) + \omega(t_{II} - t_I) + Z(\theta(t_I) + \omega(\hat{t} - t_I))\tilde{u} \mod 2\pi. \tag{22}$$

Following [14], we will proceed by using (22) as the basic building block of our control scheme. Intuitively, we want to drive the oscillator with impulses timed to occur when its phase corresponds to that of the extremal values of its PRC. For example, if the control objective is to speed up the neuron, the optimal strategy is to stimulate the neuron with a negative impulse, timed to occur when $\theta = \alpha$ (recall $Z(\alpha) = Z_{min} < 0$), followed by a positive impulse, timed to occur when $\theta = \beta$ (recall $Z(\beta) = Z_{max} > 0$).

Since we are not considering noise, we can use (22) to predict the phase of the actuated oscillator using simple algebra. The charge-balance constraint is implemented by constraining the control to be in the form of two timed impulses of equal magnitude but opposite sign. Recall that the control objective is to reduce the phase error after each period of actuation, i.e. $|\Delta\theta^+| < |\Delta\theta|$. The following control algorithm, derived using (22), gives $|\Delta\theta^+| = K|\Delta\theta|$, where we choose the desired phase error correction factor $K \in [0, 1)$:

$$u(t) = \tilde{u}(\delta(t - t_\alpha) - \delta(t - t_\beta)), \tag{23}$$

where

$$\tilde{u} = \frac{(1 - K)\Delta\theta}{Z_{max} - Z_{min}}, \qquad t_\alpha = \frac{\alpha}{\omega}, \qquad t_\beta = \frac{1}{\omega}(\beta - Z_{min}\tilde{u}). \tag{24}$$

We note here that t_α and t_β are the times at which the neuron's phase will equal α and β, respectively (see Figure 1). As in the previous sections, t represents the time since the last spiking event t^* and is reset to zero whenever θ crosses the $\theta = 2\pi \pmod{2\pi}$ spike threshold.

This control scheme is, by construction, charge balanced ("bi-phasic charge-balanced with delay" in the terminology of [28]). It corrects the error exactly as we intend over one control period, and any other control waveform would be

Corner Condition	Minimum admissible correction factor K_{min}
$0 < \theta(t_\alpha^+) < \gamma$	$1 + \frac{\alpha(Z_{max} - Z_{min})}{\pi Z_{min}}$
$\theta(t_\alpha^+) < \gamma$	$1 + \frac{(\gamma - \alpha)(Z_{max} - Z_{min})}{\pi Z_{min}}$
$\gamma < \theta(t_\beta^+)$	$1 - \frac{(\beta - \gamma)(Z_{max} - Z_{min})}{\pi Z_{max}}$
$\gamma < \theta(t_\beta^+) < 2\pi$	$1 - \frac{(2\pi - \beta)(Z_{max} - Z_{min})}{\pi Z_{max}}$

TABLE 1. Constraints on the tunable desired contraction factor K. If K is chosen to be greater than the value of the right column, the corner condition in the left column is satisfied.

using energy at a "weaker" region of the PRC, or would violate the charge-balance constraint.

We must remember, however, that the phase-reduced model is a simplified representation of a higher-dimensional conductance-based model, and thus has a shortcoming that must be addressed. The behavior of the phase-reduced model is not necessarily representative of the conductance-based model when the impulses are large enough to drive the oscillator to a phase where the sign of the PRC is different from what it was prior to the impulse. Also, if the oscillator is driven beyond the $\theta = 2\pi = 0 \pmod{2\pi}$ spike threshold, in either direction, the phase-reduced model loses relation to the conductance-based model, since a phase of zero implies a firing and an essential "reset" of the oscillator.

Since we are concerned with asymptotic convergence to a fixed frequency reference trajectory, we can easily avoid these issues by using fractional error correction with

$$0 \leq K_{min} \leq K < 1, \tag{25}$$

where K_{min} is constrained by functions of the PRC $Z(\theta)$. Table 1 lists the corner conditions for K_{min}. In the table, $\theta(t_\alpha^+)$ refers to the phase of the oscillator immediately after the impulse at $t = t_\alpha$. Likewise $\theta(t_\beta^+)$ refers to the phase immediately after the impulse at $t = t_\beta$.

By using fractional error correction and phase wrapping in our phase error definition, we provide the impulsive event-based control scheme with a way to reduce the total charge delivered over each actuation period while still retaining asymptotic convergence to the specified reference trajectory. We will now extend this concept to a more experimentally relevant context by approximating the impulses by finite magnitude pulses of non-zero duration.

3.2.2. *Quasi-impulsive control.* Using finite (small) magnitude control pulses is important in the context of stimulating real neurons, since the biological tissue exposed to the electrical stimulus can be damaged by large electrical currents. Also, the phase reduction method that generates the phase models we use makes the assumption that the input acts as a small perturbation. A digital approximation of a Dirac delta function as a rectangular spike with magnitude $\tilde{u}/dt$, where dt is equal to the sample time, works well for numerical simulation of the phase-reduced nonlinear oscillator model, but is inappropriate for use with the full-dimensional conductance-based model. Such a stimulus can instantaneously jolt the state far off

Condition	Minimum admissible control magnitude C_{min}
$0 < t_A$	$\frac{\omega\pi(1-K)}{2\alpha(Z_{max}-Z_{min})}$
$t_B < t_C$	$\max_{\Delta\theta\in(-\pi,\pi]}\left(\frac{\omega\Delta\theta(1-K)}{(\beta-\alpha)(Z_{max}-Z_{min})-Z_{min}(1-K)\Delta\theta}\right)$
$\theta(t_B) < \gamma$	$\max_{\Delta\theta\in(-\pi,\pi]}\left(\frac{-\omega(1-K)\Delta\theta}{2[(\gamma-\alpha)(Z_{max}-Z_{min})-Z_{min}(1-K)\Delta\theta]}\right)$
$\theta(t_C) > \gamma$	$\frac{\omega\pi(1-K)}{2(\beta-\gamma)(Z_{max}-Z_{min})}$
$\theta(t_D) < 2\pi$	$\max_{\Delta\theta\in(-\pi,\pi]}\left(\frac{-\omega(1-K)\Delta\theta}{2[(2\pi-\beta)(Z_{max}-Z_{min})+Z_{max}(1-K)\Delta\theta]}\right)$

TABLE 2. Constraints on the minimum admissible stimulus constraint $C = C_{min}$. If C is chosen to be greater than the value of the right column, the condition in the left column is satisfied.

its periodic orbit and yield results that are not closely approximated by the phase reduced model.

To address these issues, we develop a quasi-impulsive control that uses the same control effort as the impulsive control, but extends the duration and confines the magnitude of the impulse to be equal to a threshold C, which is chosen to be greater than or equal to a certain minimum value C_{min} which depends on the PRC, the phase error correction factor K, and the natural frequency of the phase neuron. The finite duration pulses will be stimulating the neuron at sub-extremal regions of the PRC, so the error correction of this protocol is not exact as in the impulsive case. We will show, however, that when implemented on the full-dimensional Hodgkin-Huxley neuron model, the resulting fractional error correction performance is quite close to the prescribed fractional error correction factor K from the phase-based quasi-impulsive control method.

Analogous to a time-delayed bang-bang control scheme, this method stimulates at magnitudes equal to the threshold constraint $C \geq C_{min}$, using rectangular pulses of opposite sign centered at t_α and t_β with durations such that the integral of each pulse is equal to $\tilde{u}$. Using a value of fractional error correction $K \geq K_{min}$ satisfying the conditions listed in Table 1, we propose the following control scheme:

$$u(t) = \begin{cases} 0 & , \quad \text{for} \quad 0 \leq t < t_A \\ \text{sgn}(\Delta\theta)C & , \quad \text{for} \quad t_A \leq t < t_B \\ 0 & , \quad \text{for} \quad t_B \leq t < t_C \\ -\text{sgn}(\Delta\theta)C & , \quad \text{for} \quad t_C \leq t < t_D \\ 0 & , \quad \text{for} \quad t_D \leq t \end{cases} \tag{26}$$

where

$$\begin{aligned} t_A &= t_\alpha - \tfrac{|\tilde{u}|}{2C} \quad , \quad t_B = t_\alpha + \tfrac{|\tilde{u}|}{2C} \\ t_C &= t_\beta - \tfrac{|\tilde{u}|}{2C} \quad , \quad t_D = t_\beta + \tfrac{|\tilde{u}|}{2C} \end{aligned} \tag{27}$$

and $\tilde{u}$ is as defined previously in (24). The corner conditions that determine the minimum admissible threshold constraint C_{min} are listed on Table 2. Together, these constraints ensure that the control signal always stimulates in the right direction and will yield a charge-balanced waveform. In the limit of $C \to \infty$, this scheme recovers the timing and performance of the purely impulsive control law (23).

Theorem 3.2. *For the phase-reduced neural oscillator model* $\dot{\theta} = \omega + Z(\theta)u(t)$ *where* $u(t)$ *is as defined in (26),* $Z(\theta)$ *satisfies the conditions from (3),* K *satisfies the conditions in Table 1, and* C *satisfies the conditions in Table 2, the phase error ratio over one period of actuation will be a strict contraction* ($|\frac{\Delta\theta^+}{\Delta\theta}| < 1$)*, implying global monotonic convergence of the oscillator phase* $\theta(t)$ *to the reference phase* $\theta_r(t)$*.*

Proof. First, a word on notation. When developing bounds to prove error convergence, underbars $\underline{x}$ and overbars $\bar{x}$ will denote the greatest lower and least upper bounds on the variable x, respectively. The objective of the proof is to show that the error gain, $|\frac{\Delta\theta^+}{\Delta\theta}|$, is strictly less than one for all values of initial error $\Delta\theta \in (-\pi, \pi]$. This implies that the phase error is reduced after each event-driven actuation period. And since the oscillator in absence of input rotates around $\mathbb{S}^1$ with natural frequency ω, spiking events are persistent in time, which make it impossible for a steady state error to exist.

If the extension of the impulsive control to the quasi-impulsive case were perfect, we would expect $|\frac{\Delta\theta^+}{\Delta\theta}| = K$. This, however, is the greatest lower bound, since a pulse with nonzero duration implies that the control will be stimulating the neuron at phases where the PRC will be sub-extremal. We will proceed with the proof by developing bounds on the time at which the oscillator will spike (cross the $\theta = 2\pi$ threshold), which we will denote as t^+, and which will be compared with the time at which the constant frequency reference oscillator spikes to determine the phase error after one period of actuation, $\Delta\theta^+$.

For simplicity, we will develop bounds on t^+ by separately considering the cases $\Delta\theta > 0$ and $\Delta\theta < 0$. When $\Delta\theta = 0$, no control action is taken so that $\Delta\theta^+ = 0$.

Case I: $\Delta\theta > 0$

Intuitively, the control should slow the neuron down when $\Delta\theta > 0$. A control magnitude $C \geq C_{min}$ satisfying the conditions in Table 2 guarantees that throughout the duration of the first pulse, the oscillator will have a phase between 0 and γ, the region where $Z(\theta)$ is negative semidefinite. For a positive $\Delta\theta$, the pulse will be positive, so the stimulus can only decrease the velocity of the oscillator below ω. Likewise, admissibility of the control magnitude further guarantees that the oscillator's phase will be between γ and 2π (the region where $Z(\theta)$ is positive semidefinite) during the second pulse which is negative, since $\Delta\theta > 0$. Again this means that the control signal can only decrease the oscillator's velocity below its natural frequency ω.

If there was no control, the neuron would spike again at $t^+ = 2\pi/\omega$, which would result in $\Delta\theta^+ = \Delta\theta$. In view of the argument above, this is, in fact, the lower bound $\underline{t}^+$.

Now we step through the dynamics to develop an upper bound for t^+. We begin at $\theta(0) = 0$. Then, advancing with zero input until t_A,

$$\theta(t_A) = \omega t_A = \alpha - \frac{\omega(1-K)\Delta\theta}{2C(Z_{max} - Z_{min})}.$$

Now we calculate a lower bound on $\theta(t_B)$. We do this by using Z_{min} as a lower bound on the PRC. Between t_A and t_B, our input is equal to C. We obtain

$$\begin{aligned}\underline{\theta}(t_B) &= \theta(t_A) + (\omega + Z_{min}C)(t_B - t_A) \\ &= \alpha + \frac{(\omega + 2CZ_{min})(1-K)\Delta\theta}{2C(Z_{max} - Z_{min})}.\end{aligned}$$

We then evolve with zero input until t_C:

$$\underline{\theta}(t_C) = \underline{\theta}(t_B) + \omega(t_C - t_B) = \beta - \frac{\omega(1-K)\Delta\theta}{2C(Z_{max} - Z_{min})}.$$

The input is then applied again, this time in the negative direction, since we wish to slow the neuron down, and $Z_{max} > 0$. We obtain

$$\begin{aligned}\underline{\theta}(t_D) &= \underline{\theta}(t_C) + (w - Z_{max}C)(t_D - t_C) \\ &= \beta + \frac{(\omega - 2CZ_{max})(1-K)\Delta\theta}{2C(Z_{max} - Z_{min})}.\end{aligned}$$

We now solve for the upper bound $\overline{t^+}$ using the relation

$$\theta(\overline{t^+}) = 2\pi = \underline{\theta}(t_D) + \omega(\overline{t^+} - t_D),$$

giving

$$\overline{t^+} = t_D + \frac{2\pi - \underline{\theta}(t_D)}{\omega} = \frac{2\pi + (1-K)\Delta\theta}{\omega}$$

So for $\Delta\theta > 0$,

$$\frac{2\pi}{\omega} < t^+ \leq \frac{2\pi + (1-K)\Delta\theta}{\omega}.$$

In terms of phase, these bounds on t^+ imply $K \leq \frac{\Delta\theta^+}{\Delta\theta} < 1$, as desired.

Case II: $\Delta\theta < 0$

When $\Delta\theta < 0$, the control method seeks to speed up the oscillator. Following the $C \geq C_{min}$ admissibility argument from Case I, but with the signs flipped, we conclude that the control signal cannot slow the oscillator down. Thus we have a simple upper bound: $\overline{t^+} = 2\pi/\omega$. We can now step through the dynamics in the same manner as Case I, but with $\Delta\theta < 0$, to yield the inequality

$$\frac{2\pi + (1-K)\Delta\theta}{\omega} \leq t^+ < \frac{2\pi}{\omega}.$$

Therefore, $K \leq \frac{\Delta\theta^+}{\Delta\theta} < 1$, as claimed.

Thus, for all nonzero values of $\Delta\theta \in (-\pi, \pi]$, the control provides error contraction over one period of actuation, and if $\Delta\theta = 0$, the control takes no action. □

The solid lines in the plots in Figure 4 illustrate the performance of this control algorithm for the phase-reduced model derived from the Hodgkin-Huxley system with the PRC shown previously in Figure 1. For this PRC, the minimum admissible values K_{min} and C_{min} are 0.63 and 1.65, respectively. The results shown are for $K = 0.7$ and $C = 1.7$. We see that the gain $\left|\frac{\Delta\theta^+}{\Delta\theta}\right|$ is between 0.7 and 0.8 over the entire interval, quite close to our prescribed K value of 0.7 derived from the optimal impulsive control method (23). As discussed in [13], the global stability of the origin of $M : \Delta\theta \mapsto \Delta\theta^+$ determines the global asymptotic stability of the

phase error. Here, M is well-behaved, smooth, and is confined to the first and third quadrants (as expected with global monotonic convergence), which results in global asymptotic stability of the phase error.

We now implement the quasi-impulsive control method (26) on the full-dimensional neuron model (1) using parameters listed in [7]. Our objective is to show that the phase error gain $\left|\frac{\Delta\theta^+}{\Delta\theta}\right|$ is less than one for all initial values of $\Delta\theta$. We will also compare the results to those achieved with the phase-reduced model.

Before outlining our results, we will briefly explain how we implement the control, which was developed for the phase-reduced model, on the full-dimensional model. For a single simulation, we choose an initial error $\Delta\theta$. We initialize the state of the model with phase $\theta(0) = 0$ (the state vector representation of that point on the periodic orbit, $\mathbf{x}(0)$, is known based on information derived during the phase reduction). We then integrate the ODE system (in $\mathbf{x}$ coordinate space) using the electrical stimulus signal $I(t) = cu(t)$, where we recall that c is the constant membrane capacitance (which for the standard Hodgkin-Huxley system is equal to $1.0\mu\text{F/cm}^2$). The simulation proceeds until a spike is detected (the details of spike detection and phase sampling can be found in [11]). The timing of this spike is compared to the timing of the reference oscillator spike (initialized based on the choice of $\Delta\theta$) to obtain the value of $\Delta\theta^+$.

The results of fifty individual simulations with initial conditions ranging over $\Delta\theta \in (-\pi, \pi]$ are shown as a black line with white circle markers on Figure 4. We see that the implementation of the control law based on the phase-reduced model yields very similar results for the full-dimensional system. These results represent a significant improvement over previous work [13]. Here we have monotonic error convergence, whereas previous methods yielded asymptotic error convergence of $|\frac{\Delta\theta^+}{\Delta\theta}|$, a somewhat weaker control objective.

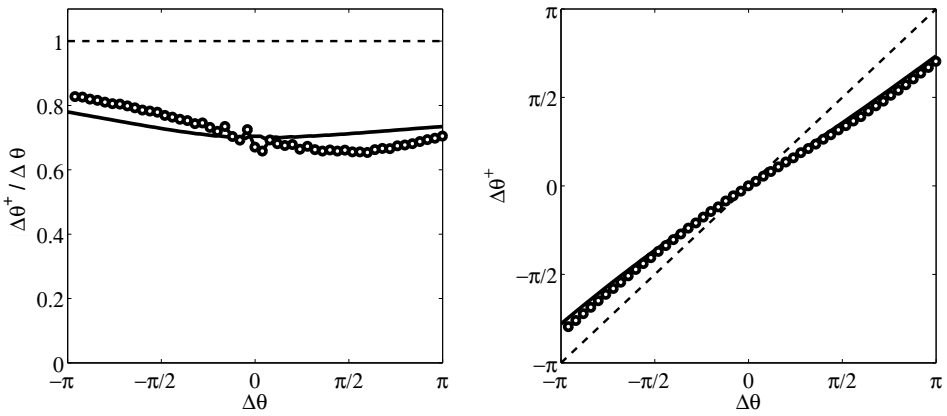

FIGURE 4. Quasi-impulsive control algorithm performance. The left plot shows the phase error gain. The right plot shows the $\Delta\theta \mapsto \Delta\theta^+$ map. Solid lines are results from the phase-reduced model to be compared with the white circle markers, which are results from the full-dimensional Hodgkin-Huxley system.

4. **Control of an ensemble of neurons.** In this section, we describe how the methods for controlling individual neurons described in the previous section might be extended to control an ensemble of neurons, including an ensemble driven by a pacemaker.

4.1. **Desynchronizing an ensemble.** Consider an ensemble of N identical uncoupled neurons firing in pathological synchrony. One can desynchronize the spike times of the ensemble using N instances of the control methods presented earlier for individual neurons.

Fully desynchronized spike times imply the population's interspike interval is constant and equal to T/N. We will first show how the energy-optimal control strategy from Section 3.1 can achieve this goal using staggered spike time targets. Then we will show how the reference-tracking methods from Sections 3.2.1 and 3.2.2 can accomplish the same goal using staggered reference phase trajectories.

4.1.1. *Energy-optimal desynchronization.* We can apply the energy-optimal methods from Section 3.1 so that each neuron has a staggered array of spike times that the controller drives it to hit. For example, label each neuron with an index $i \in \{1, \ldots, N\}$. An effective control scheme will drive each neuron i to spike at time $t_{1_i} = t + \frac{iT}{N}$ where T is the natural period of the oscillators, and t is the current time, which may be taken as zero without loss of generality. This simple arrangement sets up a staggered set of spike times that results in completely desynchronized ensemble spiking.

4.1.2. *Reference-phase tracking desynchronization.* In a similar spirit, the reference-tracking control scheme from Sections 3.2.1 and 3.2.2 can be extended to the ensemble case by using a set of staggered reference phase trajectories by setting the initial condition of each of the $i = 1, \ldots, N$ reference oscillators (20) to be $\theta_{r_i}(0) = \frac{2\pi i}{N}$. The i^{th} event-based controller then asymptotically drives its neuron toward the reference trajectory $\theta_{r_i}(t)$, resulting in asymptotic convergence to the desired desynchronized phase trajectories.

4.2. **Desynchronizing a pacemaker-driven ensemble.** In this section, we show how the reference-phase tracking methods presented in Sections 3.2.1 and 3.2.2 can be further extended to address an ensemble of neurons that are being driven towards synchrony by a periodic impulsive stimulus called a pacemaker.

4.2.1. *Pacemaker-driven ensemble model.* We consider a pacemaker-driven ensemble of N identical phase neurons depicted in Figure 5. Such a model is not directly representative of any particular biological network, but is a simple example of pathologically-driven synchronization that can be mitigated with an extension of the control methods proposed in Sections 3.2.1 and 3.2.2.

In the pacemaker-driven ensemble model, each neuron is unidirectionally coupled to a central pacemaker, and has its own event-based controller. We assume each neuron's event-based controller can both observe spikes and stimulate the neuron it controls. The pacemaker fires periodically and is not affected by either the driven neurons or any control stimuli, but its spiking can be measured and known by each controller. We also assume the pacemaker communicates with the neurons by impulsive signals.

Since the neurons do not communicate with each other, we can analyze the dynamics of this system by considering the behavior of a single pacemaker-neuron-controller system. If a controller can drive the pacemaker-driven neuron asymptotically toward a reference phase trajectory with any initial condition $\theta_{r_i}(0) \in [0, 2\pi)$, then a set of such controllers can accomplish the goal of driving each neuron toward a staggered reference phase trajectory for the ensemble.

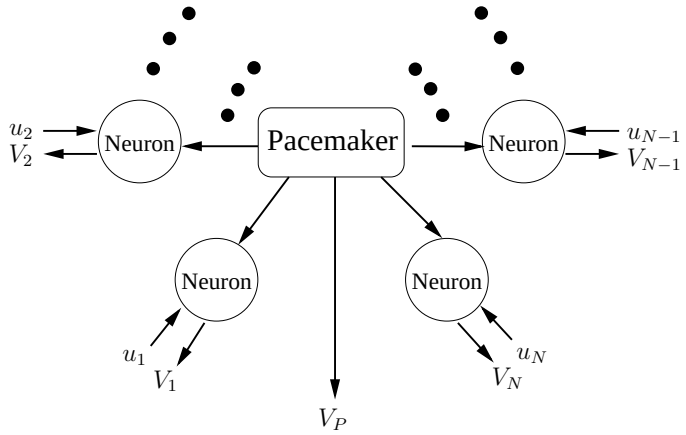

FIGURE 5. Pacemaker network. Each of the N neurons is driven by control signals u_i and the pacemaker voltage V_P. The controller observes spiking behavior of the individual neuron voltages V_i and the pacemaker voltage V_P.

We define the pacemaker as a simple oscillator

$$\dot{\theta}_P = \omega_P \quad , \quad \theta_P(0) = \theta_{P_0} \tag{28}$$

that periodically emits an impulsive signal of fixed (and known) strength K_P when its phase θ_P crosses 0, that is

$$V_P(t) = K_P \delta(\theta_P(t)). \tag{29}$$

We will take the natural frequency of the pacemaker to equal that of the phase neurons $\omega_P = \omega$. The pacemaker pulse strength K_P is taken to be positive and of order 1. Since, in this simple model, the dynamics of the pacemaker are fixed and deterministic, we can construct a simple observer that will provide the controller with an (exact) estimate of the phase of the pacemaker. The controller observes the times of two consecutive pacemaker spikes, T_{P1} and T_{P2}. Then it is possible to construct the (exact) estimated pacemaker phase trajectory:

$$\theta_P(t) = \frac{2\pi}{T_{P2} - T_{P1}}(t - T_{P2}) \mod 2\pi$$

for future times $t \geq T_{P2}$.

We model neurons as nonlinear phase oscillators that emit a detectable impulsive signal when their phase θ_i crosses 0 according to the following equation

$$\dot{\theta}_i = \omega + Z(\theta_i(t))[V_P(t) + u_i(t)], \quad \theta_i \bmod 2\pi,$$

where u_i is the control signal applied to neuron i. For each controller, we define its *event* to be the zero crossing of the phase of its controlled neuron.

4.2.2. *Uncontrolled dynamics.* For small positive pacemaker strength K_P, the spike times of the uncontrolled system synchronize with the pacemaker. This can be explained as follows. Set $t = 0$, and the first pacemaker spike occurs at time $t = T_{P1}$. Just before the spike happens, neuron i has phase $\theta_i(T_{P1}^-)$. Immediately after the spike, the phase has shifted to $\theta_i(T_{P1}^+) = \theta_i(T_{P1}^-) + K_P Z(\theta_i(T_{P1}^-)) \bmod 2\pi$. Now, the pacemaker will fire next at time $T_{P2} = T_{P1} + \frac{2\pi}{\omega}$. The neuron's phase right before the next pacemaker spike at $t = T_{P2}$ is calculated to be

$$\theta_i(T_{P2}^-) = \theta_i(T_{P1}^+) + \omega\frac{2\pi}{\omega} \mod 2\pi \quad = \theta_i(T_{P1}^+).$$

In general

$$\theta_i(T_{Pj}^-) = \theta_i(T_{P(j-1)}^+)$$

and

$$\theta_i(T_{Pj}^+) = \theta_i(T_{Pj}^-) + K_P Z(\theta_i(T_{Pj}^-))$$

which, by fixing the coupling strength K_P, can be interpreted as a one-dimensional map $M : \theta_i(T_{Pj}^-) \mapsto \theta_i(T_{Pj}^+)$ where

$$M(\theta) = \theta + K_P Z(\theta).$$

Phase entrainment is equivalent to attraction to the fixed point at the origin of the map M over the full measure of θ^- state space. In Figure 6, we have shown the map M_{HH} for the Hodgkin-Huxley phase oscillator with a rather large pacemaker strength, $K_P = 2$, for easy visualization. The origin of this map is readily verified to be asymptotically attractive on the full measure of its domain, by cobwebbing [35], for example. We note the presence of an unstable fixed point at $\theta^- = \gamma$, which is expected since $Z(\gamma) = 0$.

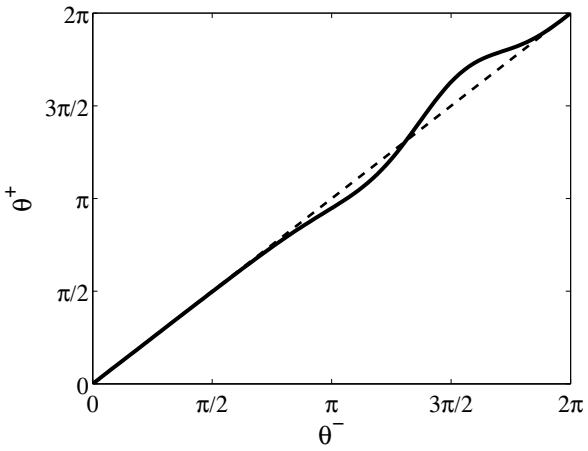

FIGURE 6. The map M_{HH} for $K_P = 2$.

4.2.3. *Impulsive desynchronization.* In the same spirit as Section 3.2.1, we propose a reference phase tracking control scheme based on impulsive inputs. When each neuron spikes, it resets its controller's own local clock $\tilde{t}_i$, and the control algorithm calculates an open loop waveform with the objective of reducing the neurons' phase error relative to a reference trajectory, evaluated when the neuron next spikes. This algorithm, however, is constructed based on the concept of using three impulses instead of two, as in Section 3.2.1. The additional impulse is timed to negate the effect of the pacemaker. The other two impulses are used to accomplish the reference phase tracking while fulfilling the charge balance requirement. In the forthcoming presentation, all times will be relative to $\tilde{t}_i$, the time since the neuron i last spiked. $\tilde{t}_P^+$ is the (relative) time when the pacemaker will spike again.

The control signal is composed of three impulses of strength $\bar{u}_{i,\alpha}$, K_P, and $\bar{u}_{i,\beta}$. These values will be defined shortly; they must satisfy

$$\bar{u}_{i,\alpha} - K_P + \bar{u}_{i,\beta} = 0, \tag{30}$$

in order to ensure charge-balance over the course of one stimulation interval.

Similar to the reference phase tracking algorithm presented in Section 3.2.1, this algorithm stimulates the phase neuron at the points of the PRC where the $Z(\theta)$ is minimal and maximal, i.e. $\theta_i = \alpha$ and $\theta_i = \beta$. The third impulse is timed to occur at exactly the same time as the pacemaker spike. Under these conditions, we calculate the (relative) time when the phase will be equal to α

$$\tilde{t}_{i,\alpha} = \frac{\alpha}{\omega}. \tag{31}$$

At $\tilde{t}_i = \tilde{t}_{i,\alpha}$, the controller applies an impulse with strength

$$\bar{u}_{i,\alpha} = \frac{K_P Z_{max} + (1-K)\Delta\theta_i}{Z_{max} - Z_{min}}. \tag{32}$$

The controller then waits until the time when the controlled neuron's phase will be at the PRC's maximal point $\theta_i = \beta$, which can be computed to be

$$t_{i,\beta} = \frac{\beta}{\omega} - \frac{Z_{min}(K_P Z_{max} + (1-K)\Delta\theta_i)}{\omega(Z_{max} - Z_{min})}. \tag{33}$$

At this time, the controller delivers an impulse with strength

$$\bar{u}_{i,\beta} = \frac{-((1-K)\Delta\theta_i + K_P Z_{min})}{Z_{max} - Z_{min}}. \tag{34}$$

The event-triggered open-loop control waveform can now be expressed as

$$u_i(\tilde{t}_i) = \bar{u}_{i,1}\delta(\tilde{t}_i - t_{i,\alpha}) - K_P\delta(\tilde{t}_i - \tilde{t}_P^+) + \bar{u}_{i,2}\delta(\tilde{t}_i - t_{i,\beta}). \tag{35}$$

This charge-balanced impulsive control scheme exactly nullifies the effect of the pacemaker and achieves the reference phase tracking with correction factor K in the same manner as the algorithm of Section 3.2.1.

4.2.4. *Quasi-impulsive desynchronization.* Similar to the single neuron case examined in Section 3.2.2, we seek to make this control method practical for application to a biological system, using finite magnitude control signals rather than impulses. In the pacemaker system, however, there are three impulses to approximate – the two phase-correcting impulses and the pacemaker-nulling impulse.

Figure 7(a) shows simulation results of this control scheme applied to a pacemaker network containing ten phase-reduced Hodgkin-Huxley neurons initialized in a completely synchronized spiking state. Figure 7(b) shows results from the same

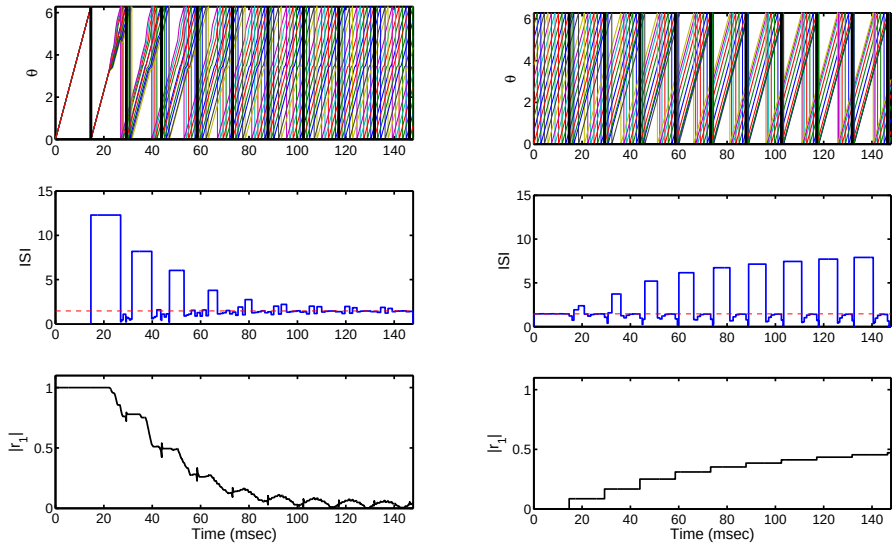

FIGURE 7. (a) Quasi-impulsive anti-pacemaker control scheme applied to a pacemaker-driven ensemble of $N = 10$ phase neurons. The spike timing of the ensemble, as well as the phase distribution, are desynchronized by the action of the controller. (b) When the controller is turned off, the pacemaker drives the ensemble back into spiking synchrony. The top panels show the time evolution of each neuron's phase. The middle panel tracks the most recent value of the ensemble's interspike interval (ISI). The bottom panels show the magnitude of the order parameter $|r_1|$.

system initialized in the desynchronized state. The phase-entraining effect of the pacemaker makes the system tend toward synchronization in absence of the controller. In these simulations, the pacemaker spike intensity was taken to be $K_P = 2$, the charge magnitude constraint on the control signal was $C = 3$ and the desired fractional error correction was $K = 0.5$. In these plots, synchrony is illustrated in two ways. The middle panels show a measure of spiking synchrony which is the time interval between the last two spikes in the ensemble. Desynchronization of spike times implies that this number is always equal to the natural period of the neuron divided by the number of neurons in the ensemble. In this case, $T/N = 1.46$ msec and is shown by the dashed red line. The other important measure of synchrony is Kuramoto's order parameter [25], the magnitude of which is a measure of phase synchrony,

$$r_1 e^{i\psi} = \frac{1}{N} \sum_{i=0}^{N} e^{i\theta_i}. \tag{36}$$

Phase synchronization implies $|r_1| \to 1$, while phase desynchronization implies $|r_1| \to 0$.

5. **Conclusion.** We have presented several event-based charge-balanced feedback control algorithms which can be applied to phase models of spiking neurons. This included controlling an individual neuron, both by finding the energy-optimal current which causes a neuron to fire at a specified time, and using impulsive and quasi-impulsive inputs to make a neuron fire asymptotically in-phase with a reference oscillator. We also described how these methods, particularly the reference-phase tracking methods, might be extended to control a ensemble of neurons, including an ensemble driven by a pacemaker.

We note that the results presented in this paper on controlling ensembles of neurons require the ability to provide different inputs to each neuron, which would be very difficult to realize experimentally. The challenge remains to develop a feedback control algorithm which desynchronizes a population of *coupled* neurons through a *single*, common input to the whole population, although there are some promising results along these lines [37, 12]. Such an algorithm might truly deliver on the promise of demand-controlled deep brain stimulation for the treatment of Parkinson's disease.

Acknowledgments. This work was supported by the National Science Foundation grant NSF-0547606, and by the Institute for Collaborative Biotechnologies under grant DAAD19-03-D004 from the U.S. Army Research Office.

REFERENCES

[1] P. Ashwin and J. Swift, *The dynamics of N weakly coupled identical oscillators*, J. Nonlin. Sci., **2** (1992), 69–108.
[2] K. J. Åström and B. Bernhardsson, *Systems with Lebesgue sampling*, in "Directions in Mathematical Systems Theory and Optimization" (eds. A. Rantzer and C. I. Byrnes), Springer, **XIII** (2003), 1–13.
[3] K. J. Åström and B. Bernhardsson, *Comparison of Riemann and Lebesgue sampling for first order stochastic systems*, in "Proceedings of the 41st IEEE Conference on Decision and Control," IEEE, (2002), 2011–2016.
[4] A. L. Benabid, P. Pollak, C. Gervason, D. Hoffmann, D. M. Gao, M. Hommel, J. E. Perret and J. De Rougemont, *Long-term suppression of tremor by chronic stimulation of the ventral intermediate thalamic nucleus*, The Lancet, **337** (1991), 403–406.
[5] P. Bressloff, *Resonantlike synchronization and bursting in a model of pulse-coupled neurons with active dendrites*, J. Comp. Neurosci., **6** (1999), 237–249.
[6] E. Brown, P. Holmes and J. Moehlis, *Globally coupled oscillator networks*, in "Perspectives and Problems in Nonlinear Science: A Celebratory Volume in Honor of Larry Sirovich" (eds. E. Kaplan, J. Marsden and K. R. Sreenivasan), Springer-Verlag, (2003), 183–215.
[7] E. Brown, J. Moehlis and P. Holmes, *On the phase reduction and response dynamics of neural oscillator populations*, Neural Comp., **16** (2004), 673–715.
[8] E. Brown, J. Moehlis, P. Holmes, E. Clayton, J. Rajkowski and G. Aston-Jones, *The influence of spike rate and stimulus duration on noradrenergic neurons*, J. Comp. Neurosci., **17** (2004), 13–29.
[9] A. Bryson and Y. Ho, "Applied Optimal Control," Halsted Press, 1975.
[10] A. Cohen, P. Holmes and R. H. Rand, *The nature of coupling between segmental oscillators of the lamprey spinal generator for locomotion: A model*, J. Math Biol., **13** (1982), 345–369.
[11] P. Danzl, R. Hansen, G. Bonnet and J. Moehlis, *Partial phase synchronization of neural populations due to random Poisson inputs*, J. Comp. Neurosci., **25** (2008), 141–157.
[12] P. Danzl, J. Hespanha and J. Moehlis, *Event-based minimum-time control of oscillatory neuron models*, Biol. Cybernet., **101** (2009), 387–399.
[13] P. Danzl and J. Moehlis, *Event-based feedback control of nonlinear oscillators using phase response curves*, in "Proceedings of the 46th IEEE Conference on Decision and Control," IEEE, (2007), 5806–5811.

[14] P. Danzl and J. Moehlis, *Spike timing control of oscillatory neuron models using impulsive and quasi-impulsive charge-balanced inputs*, in "Proceedings of the 2008 American Control Conference," IEEE, (2008), 171–176.
[15] D. B. Forger and D. Paydarfar, *Starting, stopping, and resetting biological oscillators: in search of optimal perturbations*, J. theor. Biol., **230** (2004), 521–532.
[16] W. Gerstner, L. van Hemmen and J. Cowan, *What matters in neuronal locking?*, Neural Comp., **8** (1996), 1653–1676.
[17] R. M. Ghigliazza and P. Holmes, *A minimal model of a central pattern generator and motoneurons for insect locomotion*, SIAM J. on Applied Dynamical Systems, **3** (2004), 671–700.
[18] J. Guckenheimer, *Isochrons and phaseless sets*, J. Math. Biol., **1** (1975), 259–273.
[19] D. Hansel, G. Mato and C. Meunier, *Phase dynamics for weakly coupled Hodgkin-Huxley neurons*, Europhys. Lett., **25** (1993), 367–372.
[20] A. L. Hodgkin and A. F. Huxley, *A quantitative description of membrane current and its application to conduction and excitation in nerve*, J. Physiol., **117** (1952), 500–544.
[21] F. C. Hoppensteadt and E. M. Izhikevich, "Weakly Connected Neural Networks," Springer-Verlag, New York, 1997.
[22] E. M. Izhikevich, "Dynamical Systems in Neuroscience: The Geometry of Excitability and Bursting," Springer, New York, 2007.
[23] H. K. Khalil, "Nonlinear Systems," Prentice Hall, Upper Saddle River, NJ, 2002.
[24] N. Kopell and G. B. Ermentrout, *Phase transitions and other phenomena in chains of coupled oscillators*, SIAM J. Appl. Math., **50** (1990), 1014–1052.
[25] Y. Kuramoto, "Chemical Oscillations, Waves, and Turbulence," Springer, Berlin, 1984.
[26] J. C. Lilly, G. M. Austin and W. W. Chambers, *Threshold movements produced by excitation of cerebral cortex and efferent fibers with some parametric regions of rectangular current pulses (cats and monkeys)*, J. Neurophys., **15** (1952), 319–341.
[27] J. C. Lilly, J. R. Hughes, E. C. Alvord Jr. and T. W. Galkin, *Brief, noninjurious electric waveform for stimulation of the brain*, Science, **121** (1955), 468–469.
[28] D. R. Merrill, M. Bikson and J. G. R. Jefferys, *Electrical stimulation of excitable tissue: design of efficacious and safe protocols*, J. Neuroscience Methods, **141** (2005), 171–198.
[29] R. E. Mirollo and S. H. Strogatz, *Synchronization of pulse-coupled biological oscillators*, SIAM Journal on Applied Mathematics, **50** (1990), 1645–1662.
[30] J. Moehlis, E. Shea-Brown and H. Rabitz, *Optimal inputs for phase models of spiking neurons*, ASME J. Comp. Nonlin. Dyn., **1** (2006), 358–367.
[31] A. Nabi and J. Moehlis, *Charge-balanced optimal inputs for phase models of spiking neurons*, in "Proceedings of the ASME 2009 Dynamic Systems and Control Conference," ASME, (2009), DSCC2009–2541.
[32] D. Pare, R. Curro'Dossi and M. Steriade, *Neuronal basis of the Parkinsonian resting tremor: A hypothesis and its implications for treatment*, Neuroscience, **35** (1990), 217–226.
[33] M. Schaus, "Neural Oscillator Identification via Phase-Locking Behavior," Masters thesis, University of California, Santa Barbara, 2005.
[34] T. Stigen, P. Danzl, J. Moehlis and T. Netoff, *Linear control of neuronal spike timing using phase response curves*, in "Proceedings of the 31st Annual International Conference of the IEEE EMBS," IEEE, (2009), 1541–1544.
[35] S. H. Strogatz, "Nonlinear Dynamics and Chaos: With Applications to Physics, Biology, Chemistry, and Engineering," Perseus Books, 2001.
[36] P. A. Tass, "Phase Resetting in Medicine and Biology," Springer, New York, 1999.
[37] P. A. Tass, *Effective desynchronization by means of double-pulse phase resetting*, Europhys. Lett., **53** (2000), 15–21.
[38] A. Winfree, "The Geometry of Biological Time, Second Edition," Springer, New York, 2001.
[39] A. Winfree, *Biological rhythms and the behavior of populations of coupled oscillators*, J. Theo. Biology, **16** (1967), 15–42.

Received October 2009; revised February 2010.

E-mail address: pdanzl@engineering.ucsb.edu
E-mail address: nabi@engineering.ucsb.edu
E-mail address: moehlis@engineering.ucsb.edu